A Coherent Beam Splitter for Electronic Spin States

J. R. Petta, *et al.*

Science **327**, 669 (2010);
DOI: 10.1126/science.1183628

Science (print ISSN 0036-8075; online ISSN 1095-9203) is published weekly, except the last week in December, by the American Association for the Advancement of Science, 1200 New York Avenue NW, Washington, DC 20005.

tial structure that is multifractal in nature. This property is directly related to the scale-invariant nature of critical wave functions and has been examined in great detail by numerical simulations of the single-particle quantum states near an Anderson transition (*8*). Multifractal patterns, which are ubiquitous in nature, are usually described by analysis of their self-similarity at different length scales through their singularity spectrum $f(\alpha)$. Physically, $f(\alpha)$ describes all the fractal dimensions embedded in a spatial pattern, such as those associated with a quantum wave function and its probability distribution. It is calculated by splitting the probability distribution into sets of locations $\{r_i\}$ that share a common exponent α, where the distribution scales locally with distance as $|\Psi(r_i)|^2 \sim L^{-\alpha}$, and measuring the fractal dimension of each set (*8*, *21*). A variety of techniques have been developed to compute $f(\alpha)$, which has been used to distinguish between various models of the Anderson transition (*21*, *30*). Application of such an analysis to our conductance maps (Fig. 5D, inset) shows an $f(\alpha)$ spectrum that is peaked at a value away from 2, which is indicative of anomalous scaling in a two-dimensional map. The $f(\alpha)$ spectrum also shows a systematic shift with decreasing doping, indicating a trend from weak toward strong multifractality with decreasing doping. In contrast, these signatures of multifractal behavior are absent for states deep in the valence band (gray curve) that, despite the strong disorder, show scaling consistent with those expected for extended states.

Our findings suggest that proximity to the metal-insulator transition and electronic correlations may play a more important role in the underlying mechanism of magnetism of $Ga_{1-x}Mn_xAs$ than previously anticipated. Beyond its application to understand the nature of states $Ga_{1-x}Mn_xAs$, our experimental approach provides a direct method to examine critical correlations for other material systems near a quantum phase transition. In principle, experiments at the lowest temperatures for samples closest to the metal-insulator transition should provide accurate measurements of power-law characteristics that can be directly compared to theoretically predicted critical exponents.

References and Notes

1. P. W. Anderson, *Phys. Rev.* **109**, 1492 (1958).
2. A. Lagendijk, B. van Tiggelen, D. S. Wiersma, *Phys. Today* **62**, 24 (2009).
3. A. Aspect, M. Inguscio, *Phys. Today* **62**, 30 (2009).
4. P. A. Lee, T. V. Ramakrishnan, *Rev. Mod. Phys.* **57**, 287 (1985).
5. D. Belitz, T. R. Kirkpatrick, *Rev. Mod. Phys.* **66**, 261 (1994).
6. S. Ilani *et al.*, *Nature* **427**, 328 (2004).
7. K. Hashimoto *et al.*, *Phys. Rev. Lett.* **101**, 256802 (2008).
8. F. Evers, A. D. Mirlin, *Rev. Mod. Phys.* **80**, 1355 (2008).
9. H. Ohno *et al.*, *Nature* **408**, 944 (2000).
10. D. Chiba *et al.*, *Nature* **455**, 515 (2008).
11. T. Dietl, H. Ohno, F. Matsukura, J. Cibert, D. Ferrand, *Science* **287**, 1019 (2000).
12. K. S. Burch *et al.*, *Phys. Rev. Lett.* **97**, 087208 (2006).
13. T. Jungwirth *et al.*, *Phys. Rev. B* **76**, 125206 (2007).
14. T. Dietl, *J. Phys. Soc. Jpn.* **77**, 031005 (2008).
15. C. P. Moca *et al.*, *Phys. Rev. Lett.* **102**, 137203 (2009).
16. S. H. Chun, S. J. Potashnik, K. C. Ku, P. Schiffer, N. Samarth, *Phys. Rev. B* **66**, 100408(R) (2002).
17. D. Neumaier *et al.*, *Phys. Rev. Lett.* **99**, 116803 (2007).
18. L. P. Rokhinson *et al.*, *Phys. Rev. B* **76**, 161201 (2007).
19. B. L. Sheu *et al.*, *Phys. Rev. Lett.* **99**, 227205 (2007).
20. R. C. Myers *et al.*, *Phys. Rev. B* **74**, 155203 (2006).
21. Materials and methods are available as supporting material on *Science* Online.
22. D. Kitchen, A. Richardella, J. M. Tang, M. E. Flatté, A. Yazdani, *Nature* **442**, 436 (2006).
23. J. K. Garleff *et al.*, *Phys. Rev. B* **78**, 075313 (2008).
24. J. M. Tang, M. E. Flatté, *Phys. Rev. Lett.* **92**, 047201 (2004).
25. T. O. Strandberg, C. M. Canali, A. H. MacDonald, *Phys. Rev. B* **80**, 024425 (2009).
26. B. L. Altshuler, A. G. Aronov, *Solid State Commun.* **30**, 115 (1979).
27. D. M. Basko, I. L. Aleiner, B. L. Altshuler, *Ann. Phys.* **321**, 1126 (2006).
28. I. V. Lerner, *Phys. Lett. A* **133**, 253 (1988).
29. B. L. Altshuler, V. E. Kravtsov, I. V. Lerner, *Phys. Lett. A* **134**, 488 (1989).
30. A. Chhabra, R. V. Jensen, *Phys. Rev. Lett.* **62**, 1327 (1989).

31. This work was supported by grants from Office of Naval Research, Army Research Office, the Keck Foundation, NSF, and the NSF–Materials Research Science and Engineering Center program through the Princeton Center for Complex material. P.R. acknowledges a NSF graduate fellowship.

Supporting Online Material

www.sciencemag.org/cgi/content/full/327/5966/665/DC1
Materials and Methods
Figs. S1 to S4
References

21 October 2009; accepted 5 January 2010
10.1126/science.1183640

A Coherent Beam Splitter for Electronic Spin States

J. R. Petta,[1]* H. Lu,[2] A. C. Gossard[2]

Rapid coherent control of electron spin states is required for implementation of a spin-based quantum processor. We demonstrated coherent control of electronic spin states in a double quantum dot by sweeping an initially prepared spin-singlet state through a singlet-triplet anticrossing in the energy-level spectrum. The anticrossing serves as a beam splitter for the incoming spin-singlet state. When performed within the spin-dephasing time, consecutive crossings through the beam splitter result in coherent quantum oscillations between the singlet state and a triplet state. The all-electrical method for quantum control relies on electron–nuclear spin coupling and drives single-electron spin rotations on nanosecond time scales.

Energy-level crossings, in which two quantum states cross in energy as a function of an external parameter, are ubiquitous in quantum mechanics (*1*). Coupling of the quantum states provided by tunnel coupling with strength Δ, for example, leads to hybridization of the states and results in an anticrossing with a minimum energy splitting 2Δ (*2*, *3*). Passing a quantum state through an anticrossing in the level diagram will result in a sweep-rate–dependent nonadiabatic transition probability P_{LZ}, commonly known as the Landau-Zener probability (*4*). The theory of Landau-Zener transitions can be applied to a diverse set of problems, ranging from electronic transitions in molecular collisions to chemical reactions to neutrino conversion in the sun (*5*). We apply Landau-Zener transition physics to coherently control electronic spin states in a semiconductor double quantum dot (DQD).

Semiconductor quantum dots have emerged as promising platforms for quantum control of charge and spin degrees of freedom (*6*). Considering future applications of electron spin qubits in quantum information processing, the required elementary building blocks are the exchange gate, which couples two spins, and single-spin rotations (*7*). Extremely fast 200-ps exchange gates have been demonstrated (*6*, *8*). However, coupling to the small magnetic moment of the electron (as required for single-spin rotations) is much more difficult, leading to relatively long, ~100-ns gate-operation times in GaAs quantum dots (*9*). In addition, the ac magnetic fields required for single-spin electron spin resonance (ESR) are difficult to localize on a single quantum dot (~40 nm), hindering extension of the method to a large number of quantum dots operating in close proximity. Several groups have demonstrated fast optical control of single spins, but these methods are also difficult to apply locally (*10*, *11*). In principle, local rotations can be achieved with the use of electrically driven spin resonance, which requires spin-orbit coupling and an ac electric field, but the Rabi frequencies obtained in GaAs quantum dots are approximately a factor of 2 slower than those obtained using conventional ESR (*12*, *13*). We demonstrate an all-electrical method for driving local single-spin rotations on nanosecond time scales.

Our method for coherent quantum control of electron spins is based on two consecutive sweeps through a singlet-triplet anticrossing in a DQD energy-level diagram. Coherent oscillations between the singlet and $m_s = +1$ triplet state, T_+, occur on a nanosecond time scale and are made possible by the hyperfine interaction between the trapped electron spins and the nuclear-spin bath (*14*–*16*). The oscillations are controlled by tuning the external magnetic field B_E and the voltage

[1]Department of Physics, Princeton University, Princeton, NJ 08544, USA. [2]Materials Department, University of California at Santa Barbara (UCSB), Santa Barbara, CA 93106, USA.

*To whom correspondence should be addressed. E-mail: petta@princeton.edu

pulse profile that sweeps the quantum dot system through the anticrossing in the energy-level diagram. Similar sweeps through energy-level anticrossings in superconducting qubits have been used to study Landau-Zener interference (*17*–*21*). In addition, deeply bound molecular states have been generated by transferring weakly bound Feshbach molecules through a series of anticrossings in a molecular energy manifold (*22*).

In our device (Fig. 1A), depletion gates are arranged in a triple quantum dot geometry (*23*). A DQD is formed using the middle and right dots of the device. Gate voltages V_L and V_R are used to tune the device to the (1,1)-(2,0) charge transition, where N_L and N_R indicate the number of electrons in the left and right dots, respectively. High-sensitivity charge sensing is achieved by depleting gates Q_1 and Q_2 to form a quantum point contact (QPC) charge sensor with conductance g_Q (*8*). Energy-level anticrossings (Fig. 1B) in the DQD can be used for quantum control in a manner that is directly analogous to an optical beam splitter (*18*–*20*).

The detuning, ε, of the DQD (Fig. 2A) is adjusted using V_L and V_R (*24*). For positive detuning, the ground state is the spin-singlet (2,0)S. By decreasing the detuning, a single electron can be transferred from the left dot to the right dot, forming a (1,1) charge state. Here the possible spin state configurations are the spin singlet, S, and the spin triplets T_0, T_-, and T_+ with $m_S = 0, -1$, and +1 respectively. (2,0)S and S hybridize near $\varepsilon = 0$ due to the interdot tunnel coupling T_c. The T_+ and T_- states are separated from the T_0 state by the Zeeman energy, $E_Z = g\mu_B(B_E + B_N)$, where μ_B is the Bohr magneton, and B_N is the Overhauser field ($B_N^{rms} \sim 2$ mT in the absence of nuclear polarization; rms, root mean square) (*15*). Throughout this work, we take $|g| = 0.44$, based on previous experiments (*8*, *25*). We focus on the boxed region in Fig. 2A, where hyperfine interactions mix the S and T_+ states, resulting in an anticrossing in the energy-level diagram. Under appropriate experimental conditions, we show that this anticrossing functions as a beam splitter for incoming quantum states (*18*–*20*).

We first measure the quantum state transition dynamics at the S-T_+ avoided crossing to verify the mechanism of Landau-Zener tunneling. The analytical expression for the nonadiabatic transition probability is $P_{LZ} = e^{-\frac{2\pi\Delta^2}{\hbar v}}$ (*4*). Here, $\hbar$ is Planck's constant divided by 2π, and ν is the energy-level velocity, defined as $v = |d(E_1 - E_2)/dt|$, where E_1 and E_2 are the energies of the states involved in the anticrossing. We determine Δ by measuring P_{LZ} as a function of the sweep rate through the S-T_+ anticrossing. A (2,0)S state is first prepared at positive detuning, then a rapid gate-voltage pulse (~1.1 ns, nonadiabatic with respect to the S-T_+ mixing rate) shifts the system to negative detuning ε_S, which preserves the spin singlet, S. The detuning is then increased during a ramp time T_R, sweeping the system back through the S-T_+ avoided crossing. A QPC charge sensor determines the final singlet-state probability P_S via spin-to-charge conversion (*6*).

P_S is plotted in Fig. 2B as a function of T_R. For long ramp times, the initial state should follow the adiabatic branch during the return sweep through the S-T_+ anticrossing, resulting in a final state T_+, as illustrated in the inset of Fig. 2B. We measure $P_S \sim 0.3$ at long T_R, because of the limited measurement contrast set by the spin relaxation time. At short times, P_S decays exponentially, as expected from the Landau-Zener model, with a characteristic time scale of ~180 ns. Given the detuning pulse amplitude (1.7 mV) and the conversion between gate voltage and energy [$|d(E_S - E_{T_+})/d\varepsilon| \sim 3.9$ μeV/mV], we extract a best fit $\Delta = 60$ neV (*24*). In comparison, time-resolved measurements of the S-T_+ spin-dephasing time yield $T_2^* = 10$ ns, corresponding to an energy scale of 66 neV, which is in good agreement with the value of Δ obtained above (*8*). In superconducting flux qubits, this tunnel splitting is set by tunnel junction parameters, whereas in the S-T_+ qubit, Δ is set by fluctuating transverse hyperfine fields (*15*, *18*).

Quantum control of the S and T_+ states is achieved by consecutively passing through the S-T_+ avoided crossing in the coherent limit, where the consecutive crossings take place within the spin-dephasing time (*18*–*21*). The opposite limit, where $T_R >> T_2^*$, has been shown to lead to dynamic nuclear polarization (*26*). Our pulse sequence for quantum control is illustrated in Fig. 3A and is analogous in operation to an optical interferometer (Fig. 3C, inset). An initially prepared spin-singlet state is swept through the S-T_+ avoided crossing. During this detuning sweep, the S-T_+ avoided crossing "splits" the incoming singlet state into a superposition of states S and T_+, with amplitudes A_S and A_{T_+}, analogous to an optical beam splitter. In correspondence with the Landau-Zener equation, $|A_S|^2 = P_{LZ}$. Spin angular momentum is conserved during this process by coupling to the nuclear-spin bath via the hyperfine interaction, resulting in a small

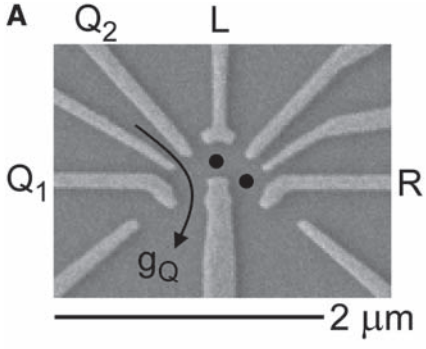

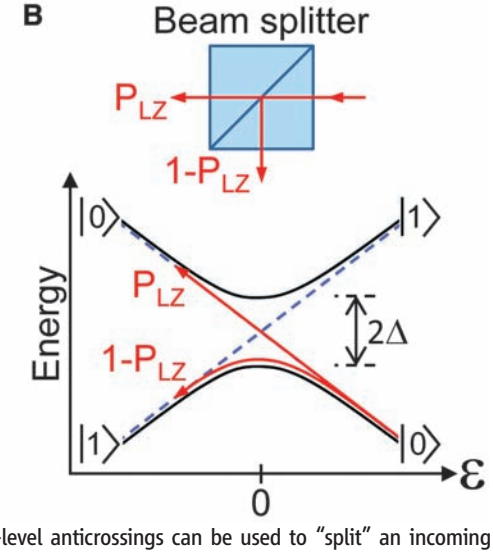

Fig. 1. (**A**) Scanning electron microscope image of a device similar to the one used in this experiment. Voltages on gates L and R tune the occupation of the DQD, whereas gates Q_1 and Q_2 form a QPC with conductance g_Q for single charge sensing. The arrow indicates the current path for the charge sensor. (**B**) Energy-level anticrossings can be used to "split" an incoming quantum state, in direct analogy with an optical beam splitter. The nonadiabatic transition probability P_{LZ} depends on the level velocity ν and the energy splitting at the anticrossing (2Δ).

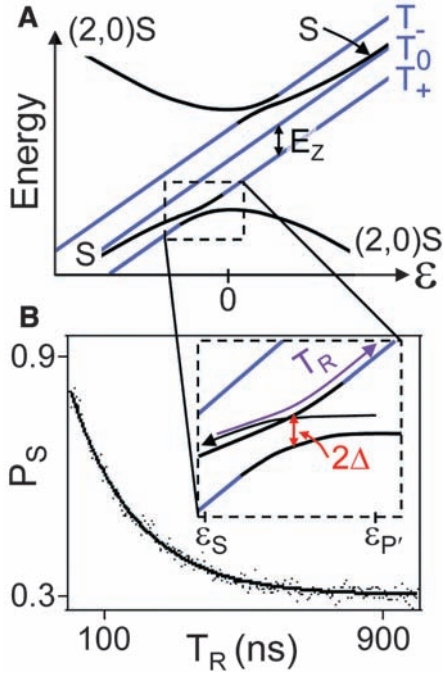

Fig. 2. (**A**) DQD energy-level diagram near the (1,1)-(2,0) charge transition. Hyperfine fields result in an anticrossing between the S and T_+ states (dashed box), which serves as a beam splitter for quantum control. (**B**) The Landau-Zener transition probability (P_{LZ}) is measured by preparing (2,0)S at positive detuning and then converting it to S via a rapid, ~1.1-ns gate-voltage–detuning pulse from $\varepsilon_{P'}$ to ε_S (here, $\varepsilon_{P'}$ is the starting value of detuning). The detuning is then increased at a constant rate from ε_S to $\varepsilon_{P'}$ during a time interval T_R, and a QPC measures P_S. The data are fit to an exponential decay (solid line), as expected from the Landau-Zener transition formula, resulting in a best fit coupling strength $\Delta = 60$ neV.

amount of nuclear polarization (*16*, *26*). Detuning is then maintained at a value ε_S for the nominal pulse length τ_S, which results in a phase accumulation $\phi = \frac{1}{\hbar}\int\{E_S[\varepsilon(t)] - E_{T_+}[\varepsilon(t)]\}dt$ (here, t is time) that is equivalent to changing the path length of one leg of an optical interferometer. A second detuning sweep takes the system back through the S-T_+ anticrossing, resulting in quantum interference of the two paths. The singlet-state return probability P_S is measured using the QPC charge sensor.

The consecutive sweeps through the S-T_+ anticrossing and the intermediate phase accumulation ϕ can be treated as unitary operations (Fig. 3B) that act on the initially prepared spin-singlet state (*4*, *27*, *28*). For the ideal case of $P_{LZ} = 1/2$, the S-T_+ anticrossing functions as a 50:50 beam splitter resulting in the unitary operator $U_1 = \frac{1}{\sqrt{2}}(\sigma_X - \sigma_Z)$, which is equivalent to a Hadamard gate (here, σ_X and σ_Z are the Pauli matrices). Phase accumulation (ϕ) during the detuning pulse results in a σ_Z rotation, $U_2 = \exp\left(\frac{-i}{2}\phi\sigma_Z\right)$, whereas the return sweep back through the S-T_+ anticrossing in the limit $P_{LZ} = 1/2$ results in a third unitary operation $U_3 = \frac{1}{\sqrt{2}}(\sigma_X - \sigma_Z)$. Functional forms for the unitary operators under general driving conditions are given in the supporting online material (*24*).

The measured P_S shows clear Stückelberg oscillations between S and T_+ as a function of τ_S and ε_S (*4*, *5*). At negative detunings, far from the avoided crossing, the oscillation period is set by $E_S - E_{T_+} = E_Z$. For B_E = 100 mT, the Zeeman energy corresponds to a period of 1.6 ns, assuming $|g|$ = 0.44, in good agreement with the ~1.5-ns period observed in the data for ε_S = –1.7 mV. The curvature of the interference pattern is partially due to the voltage pulse profile, which is smoothed to maintain some degree of adiabaticity during the sweep through the S-T_+ anticrossing. In these data (Fig. 3C), the first bright interference fringe corresponds to the condition where the detuning pulse exactly reaches the S-T_+ anticrossing. The second bright interference fringe corresponds to a configuration in which U_2 gives a 2π pulse about the z axis of the Bloch sphere.

Singlet-state probability as a function of pulse length $P_S(\tau_S)$ is plotted in Fig. 3D for two different values of detuning. The oscillation visibility ranges from 15 to 30% for these data and is a function of detuning, as the spin relaxation time

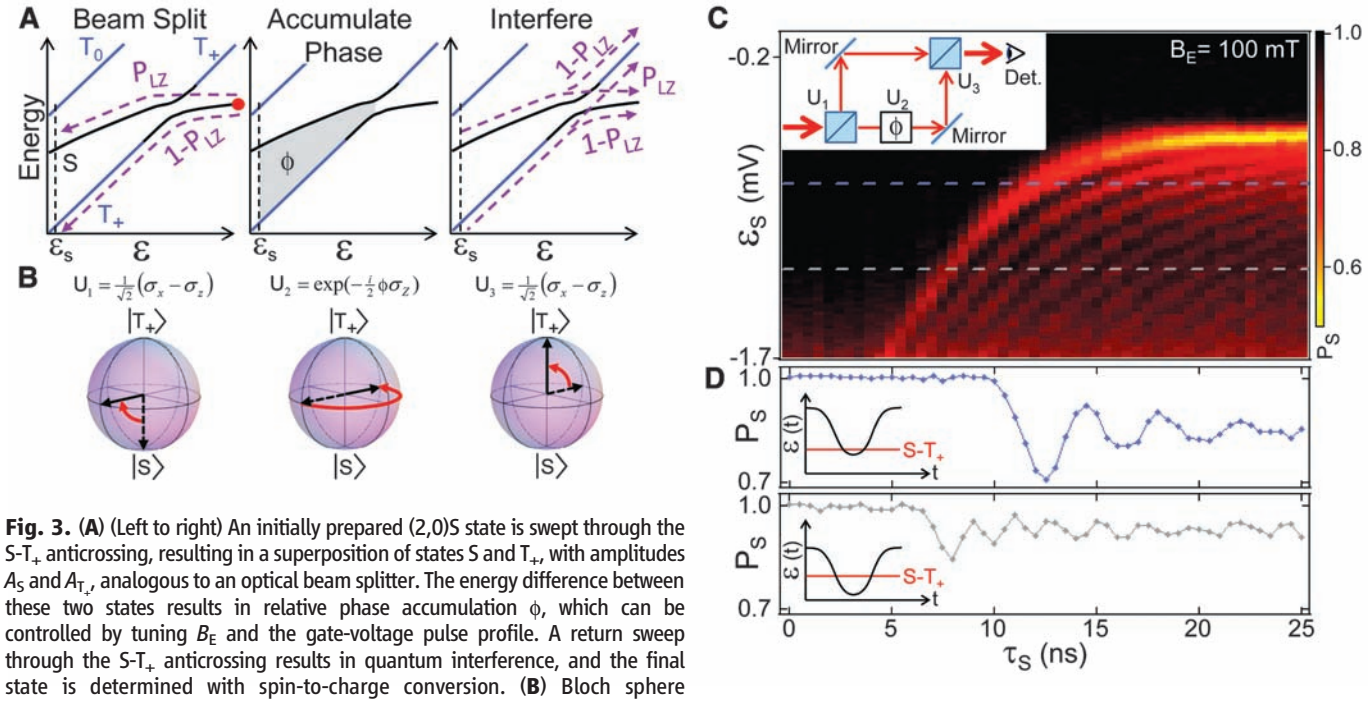

Fig. 3. (**A**) (Left to right) An initially prepared (2,0)S state is swept through the S-T_+ anticrossing, resulting in a superposition of states S and T_+, with amplitudes A_S and A_{T_+}, analogous to an optical beam splitter. The energy difference between these two states results in relative phase accumulation ϕ, which can be controlled by tuning B_E and the gate-voltage pulse profile. A return sweep through the S-T_+ anticrossing results in quantum interference, and the final state is determined with spin-to-charge conversion. (**B**) Bloch sphere representation of the unitary rotations for specific sweep conditions resulting in P_{LZ} = 1/2 and $\phi = \pi$. (**C**) P_S displays coherent oscillations as a function of separation detuning (ε_S) and pulse length (τ_S), due to Landau-Zener interference. (Inset) The experiment is equivalent to an optical interferometer, where a change in path length of one of the interferometer arms results in interference fringes as observed by a detector (Det.). (**D**) Singlet-state probability as a function of pulse length $P_S(\tau_S)$, extracted from the data in (C) for two different values of ε_S.

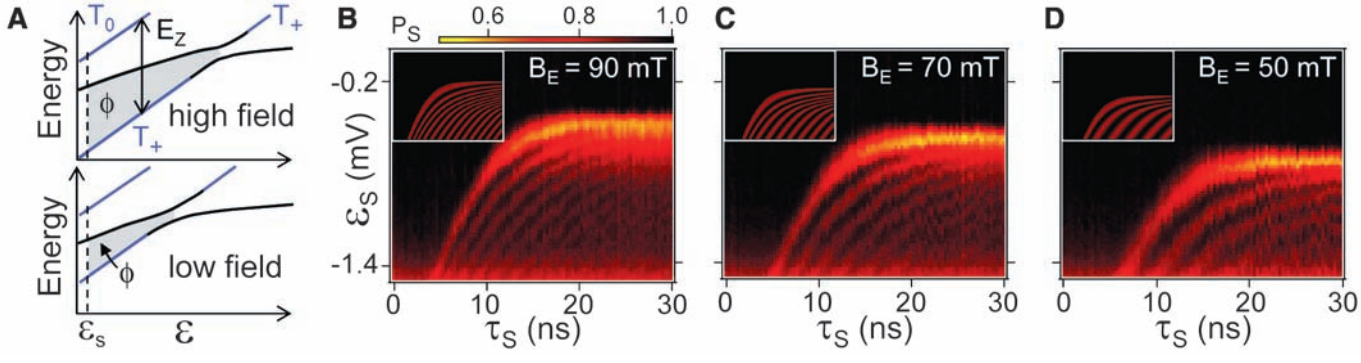

Fig. 4. (**A**) The accumulated phase ϕ is controlled by tuning B_E for a fixed set of voltage pulse parameters. A reduction in B_E shifts the position of the S-T_+ anticrossing to more negative values of ε and reduces E_S-E_{T_+}. (**B** to **D**) Measured Landau-Zener interference patterns for B_E = 90, 70, and 50 mT, respectively. (Insets) Calculated interference patterns (see text).

and P_{LZ} are detuning-dependent (*6*). Higher-visibility oscillations are obtained when the level velocity ν is small at the S-T_+ anticrossing (Fig. 3D, insets). Maximum visibility would be obtained for $P_{LZ} = 1/2$ (the limit of a perfect 50:50 beam splitter). To achieve this, detuning ramp times on the order of 160 ns >> T_2* are required, which is no longer in the coherent limit. These data suggest that active pulse shaping with subnanosecond resolution could be used to increase the fidelity of the gate operations by lowering the level velocity only in the vicinity of the S-T_+ anticrossing.

We confirm that the interference fringes are caused by consecutive sweeps through the S-T_+ beam splitter by varying B_E. Landau-Zener interference patterns are plotted in Fig. 4, B to D, for $B_E = 90$, 70, and 50 mT, respectively. A reduction in field results in two major differences: (i) The first oscillation shifts to more negative ε_S, and (ii) the oscillation frequency decreases. Both observations are consistent with the level diagram shown in Fig. 4A.

To quantitatively model the data, we calculate the probability to return to the spin-singlet state P_S by considering the action of the unitary operations (Fig. 3B) on the initially prepared spin-singlet state. Neglecting relaxation and dephasing, we find $P_S = 1 - 2P_{LZ}(1 - P_{LZ})[1 + \cos(\phi - 2\tilde{\phi}_S)]$, where $\tilde{\phi}_S$ is related to the Stoke's phase (*19*, *24*). We calculate ϕ by combining our knowledge of the voltage pulse profile with the measured $E_S(\varepsilon) - E_{T_+}(\varepsilon)$, as determined by energy-level spectroscopy (*24*). The visibility of the calculated oscillations (Fig. 4, B to D, insets) is 15% and is set by $P_{LZ} = 0.96$, as determined for these sweep conditions using the data in Fig. 2B. Overall, the observed and calculated Landau-Zener interference patterns are in very good agreement. The decay of the oscillations as a function of τ_S is most likely due to fluctuations in the Overhauser field (*8*).

Whereas commonly used single-spin rotation mechanisms rely on gigahertz frequency magnetic fields, the coherent rotations between S and T_+ demonstrated here occur on a nanosecond time scale set by the Zeeman energy and are solely driven with local gate-voltage pulses. As a result, it will be feasible to scale this quantum control method to a large number of spin qubits operating in close proximity. In addition, it is possible that the spin-flip mechanism employed here, which relies on coupling to the nuclear-spin bath, could be harnessed under the appropriate conditions to create a nuclear-spin memory (*29*).

References and Notes

1. F. Hund, *Z. Phys. A* **40**, 742 (1927).
2. J. von Neumann, E. P. Wigner, *Phys. Z.* **30**, 467 (1929).
3. R. Cohen-Tannoudji, B. Diu, F. Laloë, in *Quantum Mechanics*, vol. 1 (Wiley, New York, 1977), chap. 4.
4. S. N. Shevchenko, S. Ashhab, F. Nori, preprint available at http://arxiv.org/abs/0911.1917 (2009).
5. Y. Nakamura, *Nonadiabatic Transition* (World Scientific, London, 2001).
6. R. Hanson, L. P. Kouwenhoven, J. R. Petta, S. Tarucha, L. Vandersypen, *Rev. Mod. Phys.* **79**, 1217 (2007).
7. D. Loss, D. P. DiVincenzo, *Phys. Rev. A* **57**, 120 (1998).
8. J. R. Petta *et al.*, *Science* **309**, 2180 (2005); published online 1 September 2005 (10.1126/science.1116955).
9. F. H. L. Koppens *et al.*, *Nature* **442**, 766 (2006).
10. J. Berezovsky, M. H. Mikkelsen, N. G. Stoltz, L. A. Coldren, D. D. Awschalom, *Science* **320**, 349 (2008).
11. D. Press, T. D. Ladd, B. Y. Zhang, Y. Yamamoto, *Nature* **456**, 218 (2008).
12. K. C. Nowack, F. H. L. Koppens, Yu. V. Nazarov, L. M. K. Vandersypen, *Science* **318**, 1430 (2007); published online 1 November 2007 (10.1126/science.1148092).
13. M. Pioro-Ladrière *et al.*, *Nat. Phys.* **4**, 776 (2008).
14. W. A. Coish, D. Loss, *Phys. Rev. B* **72**, 125337 (2005).
15. J. M. Taylor *et al.*, *Phys. Rev. B* **76**, 035315 (2007).
16. H. Ribeiro, G. Burkard, *Phys. Rev. Lett.* **102**, 216802 (2009).
17. A. Izmalkov *et al.*, *Europhys. Lett.* **65**, 844 (2004).
18. W. D. Oliver *et al.*, *Science* **310**, 1653 (2005); published online 10 November 2005 (10.1126/science.1119678).
19. M. Sillanpää, T. Lehtinen, A. Paila, Y. Makhlin, P. Hakonen, *Phys. Rev. Lett.* **96**, 187002 (2006).
20. D. M. Berns *et al.*, *Nature* **455**, 51 (2008).
21. A. Izmalkov *et al.*, *Phys. Rev. Lett.* **101**, 017003 (2008).
22. F. Lang *et al.*, *Nat. Phys.* **4**, 223 (2008).
23. L. Gaudreau *et al.*, *Phys. Rev. Lett.* **97**, 036807 (2006).
24. Materials and methods are available as supporting material on *Science* Online.
25. D. M. Zumbühl, C. M. Marcus, M. P. Hanson, A. C. Gossard, *Phys. Rev. Lett.* **93**, 256801 (2004).
26. J. R. Petta *et al.*, *Phys. Rev. Lett.* **100**, 067601 (2008).
27. E. Shimshoni, Y. Gefen, *Ann. Phys.* **210**, 16 (1991).
28. A. V. Shytov, D. A. Ivanov, M. V. Feigel'man, *Eur. Phys. J. B* **36**, 263 (2003).
29. J. M. Taylor *et al.*, *Phys. Rev. Lett.* **94**, 236803 (2005).

30. We thank G. Burkard, B. Coish, D. Haldane, D. Huse, D. Loss, and H. Ribeiro for useful discussions and C. Laumann for technical contributions. Research at Princeton Univ. was supported by the Sloan Foundation, the Packard Foundation, and the NSF through the Princeton Center for Complex Materials (grant DMR-0819860) and CAREER award (grant DMR-0846341). Work at UCSB was supported by the Defense Advanced Research Projects Agency grant N66001-09-1-2020 and the UCSB National Science Foundation DMR Materials Research Science and Engineering Center.

Supporting Online Material

www.sciencemag.org/cgi/content/full/327/5966/669/DC1
Materials and Methods
SOM Text
Figs. S1 to S3
References

21 October 2009; accepted 15 December 2009
10.1126/science.1183628

Water Freezes Differently on Positively and Negatively Charged Surfaces of Pyroelectric Materials

David Ehre, Etay Lavert, Meir Lahav, Igor Lubomirsky*

Although ice melts and water freezes under equilibrium conditions at 0°C, water can be supercooled under homogeneous conditions in a clean environment down to −40°C without freezing. The influence of the electric field on the freezing temperature of supercooled water (electrofreezing) is of topical importance in the living and inanimate worlds. We report that positively charged surfaces of pyroelectric $LiTaO_3$ crystals and $SrTiO_3$ thin films promote ice nucleation, whereas the same surfaces when negatively charged reduce the freezing temperature. Accordingly, droplets of water cooled down on a negatively charged $LiTaO_3$ surface and remaining liquid at −11°C freeze immediately when this surface is heated to −8°C, as a result of the replacement of the negative surface charge by a positive one. Furthermore, powder x-ray diffraction studies demonstrated that the freezing on the positively charged surface starts at the solid/water interface, whereas on a negatively charged surface, ice nucleation starts at the air/water interface.

The ability to control the freezing temperature of supercooled water with auxiliaries, which promote or suppress ice nucleation, provides a critical factor in a variety of areas such as the survival of ectothermic animals, cryopreservation of cells and tissues, prevention of the freezing of crops, cloud seeding, and snowmaking, to mention but a few (*1*). There are a number of studies, dating back to 1861 (*2*, *3*), indicating that the local electric field near charged surfaces may enhance the freezing of supercooled water (SCW), so-called electrofreezing. This effect is attributed to the ability of the electric field to induce the formation of icelike nuclei. Electrofreezing of ice has been reported near charged metallic electrodes (*4*, *5*) or dielectric surfaces charged by mechanical friction (*6*, *7*), or within the crevices of polar crystals (*8*). X-ray specular reflectivity measurements (*9*) and vibrational spectroscopic methods such as sum-frequency generation (SFG) (*10*, *11*), supported by statistical computer simulation studies (*12*–*16*), have proposed that water molecules near surfaces in general, and near charged surfaces in particular, form clusters that are structurally different from those present in bulk water.

Studies performed with charged metallic electrodes cannot isolate the net effect of the electric field because SCW freezes at noncharged me-

Department of Materials and Interfaces, Weizmann Institute of Science, Rehovot, 76100, Israel.

*To whom correspondence should be addressed. E-mail: Igor.Lubomirsky@weizmann.ac.il